



Cite this: DOI: 10.1039/c9ob00656g

Synthesis and *in vitro* evaluation of fluorine-18 benzimidazole sulfones as CB2 PET-radioligands†

Annucca Kallinen,^a Rochelle Boyd,^b Samuel Lane,^c Rajiv Bhalla,^d Karine Mardon,^d Damion H. R. Stimson,^d Eryn L. Werry,^a Roger Fulton,^c Mark Connor ^b and Michael Kassiou ^{*a}

Cannabinoid type 2 receptor (CB2) is up-regulated on activated microglial cells and can potentially be used as a biomarker for PET-imaging of neuroinflammation. In this study the synthesis and pharmacological evaluation of novel fluorinated pyridyl and ethyl sulfone analogues of 2-(*tert*-butyl)-5-((2-fluoropyridin-4-yl)sulfonyl)-1-(2-methylpentyl)-1*H*-benzo[*d*]imidazole (**rac-1a**) are described. In general, the ligands showed low nanomolar potency (CB2 EC₅₀ < 10 nM) and excellent selectivity over the CB1 subtype (>10 000×). Selected ligands **1d**, **1e**, **1g** and **3l** showing high CB2 binding affinity (*K*_i < 10 nM) were radiolabelled with fluorine-18 from chloropyridyl and alkyl tosylate precursors with good to high isolated radioactive yields (25–44%, non-decay corrected, at the end of synthesis). CB2-specific binding of the radioligand candidates [¹⁸F]-**1d** and [¹⁸F]-**3l** was assessed on rat spleen cryosections using *in vitro* autoradiography. The results warrant further *in vivo* evaluation of the tracer candidates as prospective CB2 PET-imaging agents.

Received 21st March 2019,
Accepted 1st May 2019

DOI: 10.1039/c9ob00656g

rs.c.li/obc

Introduction

Neuroinflammation is an innate immune system response observed in a variety of central nervous system disorders including Alzheimer's and Parkinson's diseases (AD, PD), demyelinating diseases such as multiple sclerosis and traumatic brain injury.^{1–4} It is characterised by the activation of microglial cells which can differentiate into either pro- or anti-inflammatory phenotypes, often classified as M1 and M2, respectively.^{5,6} However, recent evidence suggests that the dual polarization is likely to be an over-simplification of a more dynamic system, where activated microglia represent a multitude of phenotypes, rather than two opposing functional states.⁷

Positron Emission Tomography (PET) is a non-invasive molecular imaging technique that has shown promise in detecting activated microglia and neuroinflammation in

neurodegenerative diseases.^{8–10} Microglial activation is accompanied by changes in receptor expression patterns, which offers opportunities for detecting activated cells by specific PET-radioligands. The field has largely focused on the translocator protein 18 kDa (TSPO) for the detection of *in vivo* neuroinflammation, however, TSPO imaging poses challenges, as the target is not specific for microglia but is also encountered in astrocytes.¹¹ There is also a considerable amount of TSPO present in the endothelium, which may complicate image analysis, as the signal arising from the vascular TSPO binding has to be accounted for.¹² More importantly, most of the current TSPO-radioligands show variable affinity for the target in the general population due to a common single nucleotide polymorphism (SNP) rs6971 in TSPO.^{13,14} This leads to interindividual differences in radioligand binding, which requires prior genotyping for the SNP for valid quantification of TSPO imaging.¹⁵ New PET-radioligands targeting other molecular biomarkers of activated microglia are thus needed to understand the role of microglia in neurodegeneration.

Cannabinoid receptor 2 is a G-protein coupled receptor (GPCR) which predominantly signals through Gα_{i/o} subunits. It is present in low amounts in the healthy brain, whereas a marked increase in the expression level is observed in microglia under inflammatory conditions.^{16,17} Microglial CB2 activation is considered to relate to the early neuroprotective phase of CNS inflammation, contrary to the TSPO up-regulation that is thought to occur as part of the delayed microglial

^aSchool of Chemistry, The University of Sydney, NSW 2006, Australia.
E-mail: michael.kassiou@sydney.edu.au; Tel: +612 9351 2745

^bBiomedical Sciences, Faculty of Medicine and Health Sciences, Macquarie University, NSW 2109, Australia

^cFaculty of Health Sciences, The University of Sydney, NSW 2050, Australia

^dThe Centre for Advanced Imaging, The University of Queensland, QLD 4072, Australia

† Electronic supplementary information (ESI) available. See DOI: 10.1039/c9ob00656g

activation in a pro-inflammatory fashion.^{18–20} Specific CB2 radioligands could be used as radiopharmacological tools to investigate pathophysiological mechanisms in the earliest phases of neuroinflammation, and to potentially image a different pool of microglia, thus complementing data gathered with TSPO radioligands.

There have been several CB2 PET-radioligands developed to date (Fig. 1). Despite these efforts, no candidates have progressed from the preclinical and clinical development phases into routine clinical use. 2-Oxoquinoline [¹¹C]NE40 is the first CB2-radioligand with promising pharmacokinetic properties, and has been evaluated in clinical studies in healthy volunteers and AD patients (Fig. 1).^{21,22} However, [¹¹C]NE40 was found not to accumulate in the β -amyloid deposits, and no co-localisation of CB2 and amyloid deposits could be observed.²² 4-Oxoquinoline [¹¹C]RS-016 was observed to have CB2-specific binding in LPS-induced neuroinflammation model in mice, however, the compound was suspected to suffer from poor blood–brain barrier permeability.²³ Pyridine [¹¹C]RSR-056 showed increased brain uptake under inflammatory conditions in LPS mouse model, however, only part of the binding was found to be CB2-specific.²⁴ In the initial studies, thiazole [¹¹C]A-836339 was observed to have CB2-specific binding in AD mouse model, but failed to show increased uptake in the inflammation area in animal models of neuroinflammation and in cerebral ischemia.²⁵ Triazine based ligand [¹⁸F]-19, on the other hand, was found to suffer from rapid metabolism and elimination, hindering its use as a CB2-radioligand.²⁶ Oxadiazole [¹⁸F]MA3 was recently evaluated in non-human primates and was found to have moderate uptake and washout from the brain, but CB2-specific binding could not be observed.²⁷ CB2-radioligands developed so far have been recently reviewed, providing a thorough update on the topic.²⁸

CB2 receptors also represent a largely unexploited drug target that has attracted recent interest.^{29,30} Selective CB2-agonists attenuate pro-inflammatory cytokine release and migratory activity of immune system cells in several animal

models of inflammation, and in models of AD and PD.^{31,32} The neuroprotective and anti-inflammatory effects of CB2-agonists may thus offer a new therapeutic approach for the treatment of neurodegenerative diseases. A CB2-specific PET-radioligand would also be of great importance in the evaluation of the efficacy of novel CB2-based therapeutics.

Sulfonyl benzimidazole-based CB2-agonists were originally reported by Pfizer and Janssen in the late 2000s.^{33,34} To the best of our knowledge, benzimidazole-based ligands have not been evaluated as CB2-radioligands thus far. In this study, we describe the design and synthesis of new fluorinated benzimidazole sulfones and their *in vitro* pharmacological characterisation. Selected ligands were ¹⁸F-radiolabelled as candidate radioligands and evaluated for the specific binding on rat spleen cryosections using *in vitro* autoradiography.

Results and discussion

Synthesis and *in vitro* evaluation of the fluorinated benzimidazole 5-sulfones

The lead compound *rac*-1a (Scheme 1) was selected from the patent literature, as it has been reported to have high potency at hCB2 (EC₅₀ 0.26 nM) and excellent selectivity over hCB1 subtype (EC₅₀ hCB1/hCB2 >38 900) in an assay measuring the inhibition of forskolin induced cAMP production (CHO-K1 cell line).³⁴ It was noted that the lead structure contains an electron deficient pyridine ring with fluoro-substituent in 2-position that was proposed to readily undergo S_NAr, making the incorporation of ¹⁸F facile in the structure. As ethyl sulfone benzimidazoles have shown potential for good brain uptake, we also included aliphatic 2-fluoroethyl sulfones (2) in the screening.³⁵ N1-2-Fluoroethoxyethyl chain was proposed as an alternative position for the incorporation of ¹⁸F-radiolabel in the ethyl sulfone structures (derivative 3i). This was surmised to result in potentially improved stability, as primary aliphatic ¹⁸F-substituents β to a heteroatom have been reported to

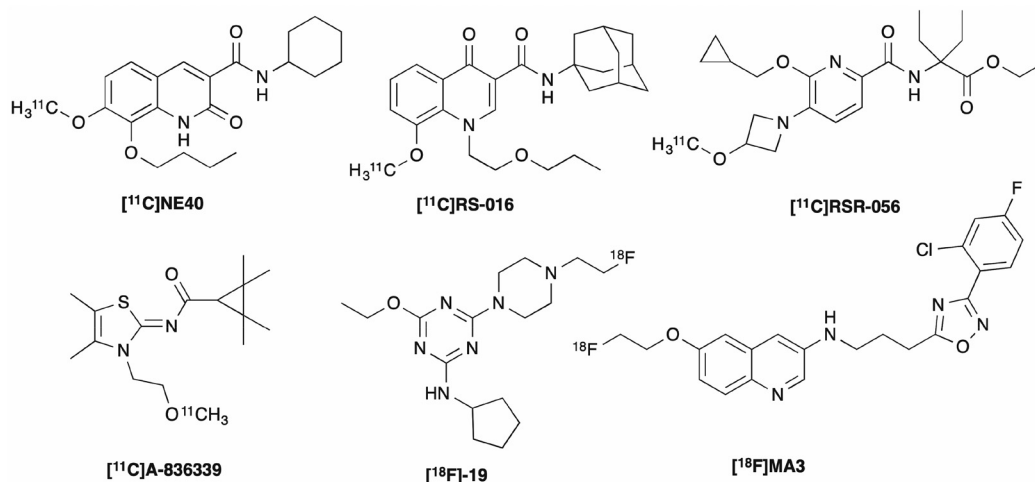
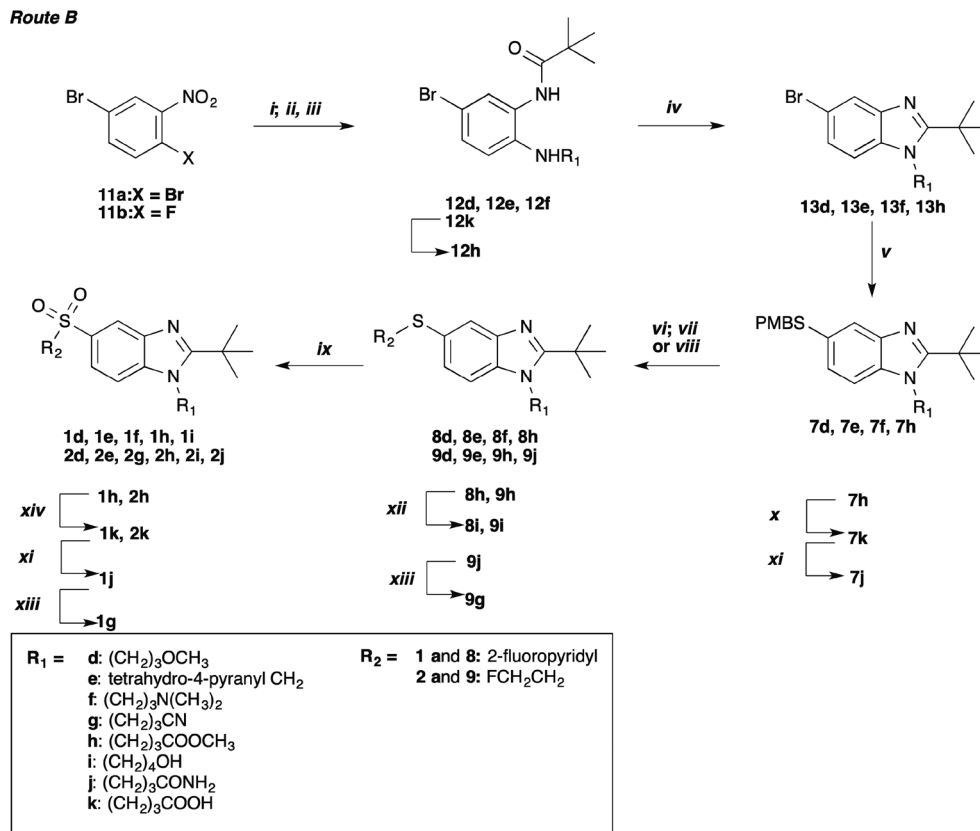


Fig. 1 Examples of recent CB2-radioligands: [¹¹C]NE40, [¹¹C]RS-016, [¹¹C]RSR-056, [¹¹C]A-836339, [¹⁸F]-19 and [¹⁸F]MA3.



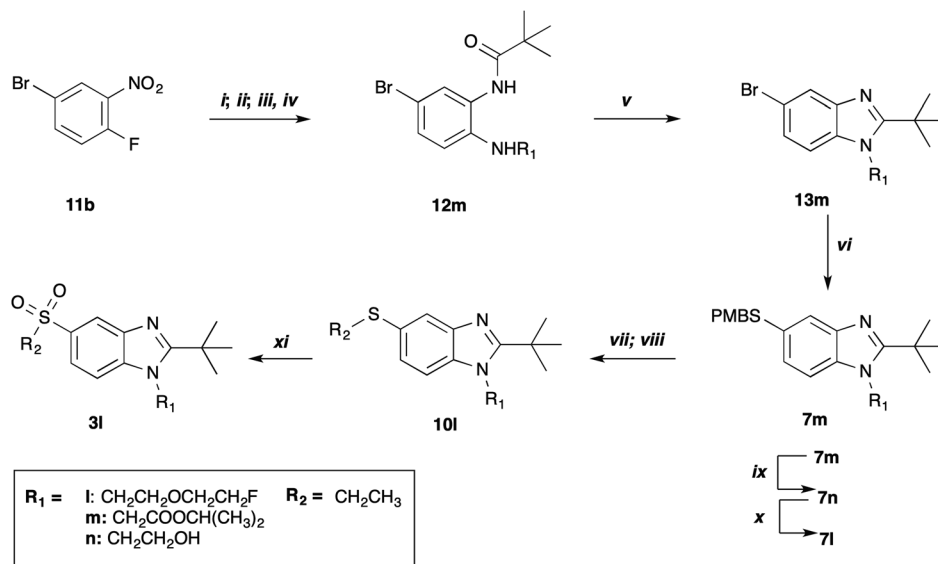
Scheme 2 Synthetic pathway B to make fluorinated benzimidazole sulfones **1** and **2**. Reagents and conditions: (i) NHR₁, DIPEA, ethanol, 100 °C (38–89%); (ii) Fe, NH₄Cl, ethanol, 40 °C (82–95%); (iii) pivaloyl chloride, pyridine, DMAP, DCM, RT (68–98%); (iv) *p*-TsOH, toluene or DMF, 130 °C (58–90%); (v) 4-methoxy- α -toluenethiol, Pd₂(dba)₃, Xantphos, DIPEA, dioxane, 90 °C (44–91%); (vi) TFA, 80 °C; (vii) 2-fluoro-4-bromopyridine, Pd₂(dba)₃, Xantphos, Cs₂CO₃, toluene, 110 °C (38–86% over 2 steps); (viii) 2-fluoroethylbromide, Cs₂CO₃, dioxane, 50 °C (42–80% over 2 steps); (ix) *m*-CPBA, DCM, 0 °C → RT (avg. 72%) or KHSO₅·1/2KHSO₄·1/2K₂SO₄, methanol, H₂O, 0 °C → RT (54%); (x) LiOH, THF/MeOH/H₂O, RT (96%); (xi) CDI, NH₄Cl, DIPEA, DMF, RT (70–85%); (xii) DIBAL-H, THF, –78 °C → RT (avg. 97%); (xiii) TFAA, TEA, DCM, 0 °C → RT (82–91%); (xiv) trimethyltinhydroxide, 1,2-DCE, 80 °C (83–88%).

The synthesis of analogue **3l** followed the same steps as described in Scheme 2 with some modifications. Here, pivalamide intermediate **12m** was prepared in 61% yield in a four-step telescoped process starting from **11b** and glycine (Scheme 3). The carboxylic acid was protected as a bulky isopropyl ester to slow down the intramolecular trans-lactamisation with the aniline in the subsequent step. *p*-TsOH catalysed condensation of the dianiline **12m** was carried out in DMSO at 100 °C to give **13m** which underwent Pd-catalysed C–S coupling with 4-methoxy- α -toluenethiol to afford **7m**. The isopropyl ester was reduced by DIBAL-H to give 2-hydroxy ethyl chain (**7n**). The pendant hydroxyl group was then subjected to *O*-alkylation with 2-fluoroethyl bromide to give an intermediate **7l**. Deprotection, followed by *S*-alkylation, gave the sulfide **10l** that was lastly oxidised to sulfone **3l**.

The ligands were evaluated for their functional activity in a fluorometric membrane potential assay that measures the activation of G-protein-coupled inwardly rectifying potassium channels (GIRKs) in an AtT-20 cell line. This was done to study the intrinsic activity of the compounds, as agonist and antag-

onist radioligands may interact with and detect different receptor pools *in vivo*.³⁹ The lead compound **rac-1a** was confirmed to act as an agonist with similar high efficacy (E_{\max} 89%) to the standard CP-55940 (Table 1). **rac-1a** had a good, but slightly lower potency at CB2 in this assay (EC_{50} = 3.5 nM) when compared to earlier data (EC_{50} = 0.26 nM).³⁴ The apparent selectivity over CB1 subtype (240 \times) was significantly lower than the value reported earlier (>38 900 \times).³⁴ It is to be noted though, that the lead compound was measured here as a racemate, and the information on the stereochemical purity was not disclosed in the previous reports.³⁴ The apparent CB2/CB1 selectivity of compounds in functional assays also depends on the relative amount of receptors expressed in each cell line, and so direct comparisons between different experiments are difficult.

The N1-alkyl chain variants (**a–c**) were included in the first screening to gauge whether the potency and selectivity is affected by the geometry of the N1-alkyl chain (Table 1). Both the flexible, linear side chain and the conformationally restricted cyclobutyl ring resulted in low nanomolar potency at CB2 in the membrane potential assay. Typically, non-opti-



Scheme 3 Synthesis of fluorinated benzimidazole sulfone **3l**. Reagents and conditions: (i) Glycine, DIPEA, ethanol, 100 °C; (ii) iPrOH, H₂SO₄, 60 °C; (iii) Fe, NH₄Cl, ethanol, 40 °C or sonication at RT; (iv) pivaloyl chloride, pyridine, DMAP, DCM, RT (61% over four steps); (v) *p*-TsOH, DMSO, 100 °C (74%); (vi) 4-methoxy- α -toluenethiol, Pd₂(dba)₃, Xantphos, DIPEA, dioxane, 90 °C (84%); (vii) TFA, 80 °C; (viii) ethylbromide, TBAI, NaOH (aq.), MeOH, 60 °C (99% over two steps); (ix) DIBAL-H, THF, -78 °C \rightarrow RT (avg. 88%); (x) 2-fluoroethylbromide, NaH, THF, 60 °C (avg. 76%); (xi) *m*-CPBA, DCM, 0 °C \rightarrow RT (72%).

Table 1 Activity of fluorinated benzimidazole sulfones with chains a–c at CB1 and CB2 in fluorometric membrane potential assay

Compd	R ₁ R ₂	CB1		CB2		SI ^b	clog P ^d	tPSA ^e (Å ²)
		pEC ₅₀ ± SEM (EC ₅₀ nM)	E _{max} ± SEM ^a (% CP 55940)	pEC ₅₀ ± SEM (EC ₅₀ nM)	E _{max} ± SEM ^a (% CP 55940)			
1a	R ₁ : <i>rac</i> -CH ₂ CH(CH ₃)(CH ₂) ₂ CH ₃ R ₂ : 2-Fluoropyridyl	6.07 ± 0.66 (843)	0.51 ± 0.22 (48)	8.46 ± 0.30 (3.5)	0.91 ± 0.09 (89)	241	5.35	62.1
1b	R ₁ : (CH ₂) ₄ CH ₃ R ₂ : 2-Fluoropyridyl	d.n.c. ^c	d.n.c.	8.05 ± 0.14 (9.0)	0.98 ± 0.05 (96)	>10 000	4.95	62.1
1c	R ₁ : <i>c</i> -Butyl CH ₂ R ₂ : 2-Fluoropyridyl	d.n.c.	d.n.c.	8.49 ± 0.12 (3.3)	0.97 ± 0.04 (95)	>10 000	4.36	62.1
2a	R ₁ : <i>rac</i> -CH ₂ CH(CH ₃)(CH ₂) ₂ CH ₃ R ₂ : 2-Fluoroethyl	d.n.c.	d.n.c.	8.50 ± 0.15 (3.1)	0.94 ± 0.05 (92)	>10 000	4.73	49.7
2b	R ₁ : (CH ₂) ₄ CH ₃ R ₂ : 2-Fluoroethyl	6.48 ± 0.27 (333)	0.59 ± 0.10 (57)	8.65 ± 0.15 (2.2)	0.89 ± 0.05 (87)	149	4.33	49.7
2c	R ₁ : <i>c</i> -Butyl CH ₂ R ₂ : 2-Fluoroethyl	d.n.c. (20 840)	d.n.c.	8.37 ± 0.11 (4.3)	0.99 ± 0.04 (97)	>4900	3.75	49.7

^a Ligand efficacy given as maximum response E_{max} ± standard error of the mean, and as intrinsic activity compared to 1 μM CP-55940.

^b Selectivity index given as a ratio EC₅₀ hCB1/EC₅₀ hCB2. ^c d.n.c. = data not converted, EC₅₀ > 10 μM. ^d clog P values were predicted with ChemDraw Professional version 15.0.0.107, BioByte fragment based method. ^e Topological polar surface area, calculated with ChemDraw Professional version 15.0.0.107.

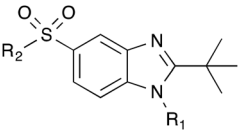
mised cannabinoid receptor agonists suffer from high lipophilicity. Accordingly, predicted lipophilicity of the lead *rac*-**1a** (clog P 5.35, ChemDraw Professional version 15.0.0.107, BioByte fragment based method) exceeds the optimal range (clog P 2–4) for CNS-targeted ligands.⁴⁰ Too high lipophilicity may result in high non-specific binding to plasma proteins,

reducing the free fraction of radioligand available for crossing BBB and binding to the target.³⁹ According to previously reported studies, bulky and lipophilic *tert*-butyl group in the 2-position of the imidazole ring is optimal for the activity.^{34,41} To reduce lipophilicity, H-bond acceptor and donor groups were introduced to the N1-substituent.

Hydrogen bond acceptors. We initially tested linear methoxy propyl, linear *N,N*-dimethylamino propyl and bulky tetrahydro-4-pyranyl methyl side chains in the *N1*-area (Table 2). The linear methoxy propyl and *N,N*-dimethylamino propyl side chains resulted in excellent CB2 subtype selectivity (>10 000×), whereas the bulky tetrahydro-4-pyranyl methyl derivatives (**1e** and **2e**) showed micromolar activities at CB1 receptor, lowering the selectivity ratio to 100–200×. It is possible that increased steric bulk of the tetrahydropyranyl moiety may result in binding at both CB1 and 2, whereas linear chains may confer better CB2 selectivity. In general, all the ligands tested showed low nanomolar potency at CB2. Of the pyridyl derivatives, **1d** had the highest potency ($EC_{50} = 3.7$ nM) and apparent selectivity over CB1 (>10 000×). Accordingly, the ethyl sulfone analogue **3l** with an isosteric ethoxy ethyl chain was found to have high activity at CB2 ($EC_{50} = 5.1$ nM) and excellent selectivity over CB1 (>10 000×). Since the methoxy group is potentially metabolically labile, analogues for methoxypropyl chain with similar bioactivity were sought from the literature database (SwissBioIsostere®). This prompted us to include the propyl nitriles (**1g** and **2g**) in the screening. Gratifyingly, **1g** also showed promise as a highly selective (ratio >10 000×) and potent ($EC_{50} = 3.0$ nM) CB2-ligand.

Hydrogen bond donors. According to Verbist *et al.*, the *N1*-substituent in benzimidazole 5-sulfones fits in a hydrophobic binding site and only H-bond acceptors are tolerated.⁴¹ In the previous studies on indole cannabinoids, terminal hydroxyl group at *N1*-alkyl chain has been observed to increase the CB2 potency and selectivity over CB1.^{42–44} Also in this series, 4-hydroxybutyl substituent resulted in nanomolar potency at CB2 ($EC_{50} = 8.6$ nM and 37 nM for **1i** and **2i**, respectively) with excellent CB2-subtype selectivity (>10 000×) (Table 3). However, conspicuous decrease in CB2 activity was associated with primary carboxamide (**1j** and **2j**) and furthermore, in carboxylic acid H-bond donors (**1k** and **2k**). The same observation has been reported with indole cannabinoids.^{42,43} It is to be noted though, that the binding orientation of the ligands is likely to vary, and more than one plausible binding site may exist, complicating the comparison of the SAR-data between different ligand classes.⁴⁵ The potency for CB2 was regained by removing the H-bond donor functionality, as seen in the methyl ester analogues (**1h** and **2h**, Table 2). When comparing the matched pairs across the H-bond acceptor and donor series, the fluoroethyl sulfones showed, in general, lower CB2 potency than 2-fluoropyridyl sulfones.

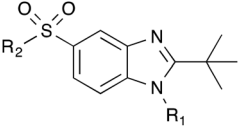
Table 2 Activity of fluorinated benzimidazole sulfones with chains **d–h** and **l** at CB1 and CB2 in fluorometric membrane potential assay



Compd	R ₁ R ₂	CB1		CB2		SI ^b	clog P ^d	tPSA ^e (Å ²)
		pEC ₅₀ ± SEM (EC ₅₀ nM)	E _{max} ± SEM ^a (% CP 55940)	pEC ₅₀ ± SEM (EC ₅₀ nM)	E _{max} ± SEM ^a (% CP 55940)			
1d	R ₁ : (CH ₂) ₃ OCH ₃ R ₂ : 2-fluoropyridyl	d.n.c. ^c	d.n.c.	8.43 ± 0.02 (3.7)	1.06 ± 0.02 (105)	>10 000	3.05	71.3
1e	R ₁ : Tetrahydro-4-pyranyl CH ₂ R ₂ : 2-Fluoropyridyl	5.97 ± 0.04 (1064)	1.01 ± 0.03 (100)	8.28 ± 0.02 (5.2)	1.06 ± 0.01 (104)	204	3.08	71.3
1f	R ₁ : (CH ₂) ₃ N(CH ₃) ₂ R ₂ : 2-Fluoropyridyl	d.n.c.	d.n.c.	8.07 ± 0.07 (8.4)	1.00 ± 0.04 (98)	>10 000	3.20	65.3
1g	R ₁ : (CH ₂) ₃ CN R ₂ : 2-Fluoropyridyl	d.n.c.	d.n.c.	8.52 ± 0.04 (3.0)	1.06 ± 0.02 (106)	>10 000	2.63	85.9
1h	R ₁ : (CH ₂) ₃ COOCH ₃ R ₂ : 2-Fluoropyridyl	d.n.c.	d.n.c.	8.17 ± 0.04 (6.7)	1.01 ± 0.02 (101)	>10 000	3.23	88.4
2d	R ₁ : (CH ₂) ₃ OCH ₃ R ₂ : 2-Fluoroethyl	d.n.c.	d.n.c.	7.77 ± 0.04 (17)	1.04 ± 0.03 (103)	>10 000	2.44	59.0
2e	R ₁ : Tetrahydro-4-pyranyl CH ₂ R ₂ : 2-Fluoroethyl	6.31 ± 0.04 (486)	1.06 ± 0.03 (105)	8.36 ± 0.05 (4.3)	1.07 ± 0.03 (105)	112	2.47	59.0
2g	R ₁ : (CH ₂) ₃ CN R ₂ : 2-Fluoroethyl	d.n.c.	d.n.c.	8.05 ± 0.04 (8.9)	1.03 ± 0.02 (102)	>10 000	2.01	73.5
2h	R ₁ : (CH ₂) ₃ COOCH ₃ R ₂ : 2-Fluoroethyl	d.n.c.	d.n.c.	8.07 ± 0.09 (8.6)	1.06 ± 0.05 (105)	>10 000	2.61	76.0
3l	R ₁ : CH ₂ CH ₂ OCH ₂ CH ₂ F R ₂ : Ethyl	d.n.c.	d.n.c.	8.29 ± 0.11 (5.1)	1.02 ± 0.05 (100)	>10 000	2.53	59.0

^a Ligand efficacy given as maximum response $E_{max} \pm$ standard error of the mean, and as intrinsic activity compared to 1 μ M CP-55940.

^b Selectivity index given as a ratio EC_{50} hCB1/ EC_{50} hCB2. ^c d.n.c. = data not converted, $EC_{50} > 10$ μ M. ^d clog P values were predicted with ChemDraw Professional version 15.0.0.107, BioByte fragment based method. ^e Topological polar surface area, calculated with ChemDraw Professional version 15.0.0.107.

Table 3 Activity of fluorinated benzimidazole sulfones with chains i–k at CB1 and CB2 in fluorometric membrane potential assay


Compd	R ₁ R ₂	CB1		CB2		SI ^b	clog P ^d	tPSA ^e (Å ²)
		pEC ₅₀ ± SEM (EC ₅₀ nM)	E _{max} ± SEM ^a (% CP 55940)	pEC ₅₀ ± SEM (EC ₅₀ nM)	E _{max} ± SEM ^a (% CP 55940)			
1i	R ₁ : (CH ₂) ₄ OH R ₂ : 2-Fluoropyridyl	d.n.c. ^c	d.n.c.	8.06 ± 0.06 (8.6)	1.06 ± 0.04 (106)	>10 000	2.43	82.3
1j	R ₁ : (CH ₂) ₃ CONH ₂ R ₂ : 2-Fluoropyridyl	d.n.c.	d.n.c.	6.98 ± 0.08 (105)	1.06 ± 0.04 (105)	>10 000	2.01	105.2
1k	R ₁ : (CH ₂) ₃ COOH R ₂ : 2-Fluoropyridyl	d.n.c.	d.n.c.	5.58 ± 0.08 (2630)	1.04 ± 0.07 (104)	>10 000	2.80	99.4
2i	R ₁ : (CH ₂) ₄ OH R ₂ : 2-Fluoroethyl	d.n.c.	d.n.c.	7.43 ± 0.04 (37)	1.05 ± 0.02 (104)	>10 000	1.82	70.0
2j	R ₁ : (CH ₂) ₃ CONH ₂ R ₂ : 2-Fluoroethyl	d.n.c.	d.n.c.	6.28 ± 0.09 (520)	0.96 ± 0.06 (95)	>10 000	1.40	92.8
2k	R ₁ : (CH ₂) ₃ COOH R ₂ : 2-Fluoroethyl	d.n.c.	d.n.c.	d.n.c.	d.n.c.	N/A	2.18	87.0

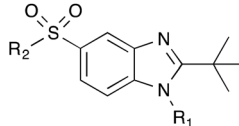
^a Ligand efficacy given as maximum response $E_{max} \pm$ standard error of the mean, and as intrinsic activity compared to 1 μ M CP-55940.

^b Selectivity index given as a ratio EC₅₀ hCB1/EC₅₀ hCB2. ^c d.n.c. = data not converted, EC₅₀ > 10 μ M. ^d clog P values were predicted with ChemDraw Professional version 15.0.0.107, BioByte fragment based method. ^e Topological polar surface area, calculated with ChemDraw Professional version 15.0.0.107.

Overall, the control ligands **rac-1a**, **1c** and **1e**, showed lower CB2-potency and subtype selectivity in the GIRK-based assay, as compared to the values reported earlier in the assay measuring cAMP inhibition.³⁴ However, in general, functional activity data is highly dependent on the assay conditions, cell line used and the secondary messenger system used to measure the receptor activation, and such data from different laboratories are difficult to compare.

Based on the functional activity screening, a few of the ligands were selected further for the radiolabelling studies. Potency, selectivity, lipophilicity and topological polar surface area of the compounds were considered. Of the pyridyl sulfones, **1d** (EC₅₀ = 3.7 nM, clog P = 3.05, tPSA = 71.3) and **1g** (EC₅₀ = 3.0 nM, clog P = 2.63, tPSA = 85.9) were selected due to their low nanomolar potency and excellent subtype selectivity. Despite the lower subtype selectivity, the pyridyl sulfone analogue **1e** (EC₅₀ = 5.2 nM, clog P = 3.08, tPSA = 71.3) was included as a back-up ligand with potentially different pharmacokinetic properties. 2-Fluoroethyl sulfone **2e** (clog P = 2.47, tPSA = 59.0) and ethyl sulfone **3l** (clog P = 2.53, tPSA = 59.0) were chosen from the alkyl sulfone series due to their high potency (EC₅₀ = 4.3 nM and 5.1 nM, respectively). The clog P and tPSA values of the candidate ligands are within the range of optimal lipophilicity (clog P 2–4) and topological polar surface area (tPSA < 90 Å²) set for passive entry into CNS, further supporting the selection of these compounds.⁴⁰

Next, the selected ligands were investigated for their binding affinity towards CB2. Competitive binding of the ligands was measured against a known radioligand standard [³H]CP-55940, a non-selective cannabinoid receptor agonist.⁴⁶

Table 4 Apparent binding affinities (K_i) of the compounds **1d**, **1g**, **1e**, **2e** and **3l**. K_i values were measured after competitive displacement of 2 nM (CB2) or 3 nM (CB1) of [³H]CP-55940


Compd	R ₁ R ₂	K_i CB1 (nM)	K_i CB2 (nM)
1d	R ₁ : (CH ₂) ₃ OCH ₃ R ₂ : 2-Fluoropyridyl	>10 000	2.6 ± 1.0
1g	R ₁ : (CH ₂) ₃ CN R ₂ : 2-Fluoropyridyl	>10 000	3.5 ± 1.7
1e	R ₁ : Tetrahydro-4-pyranyl CH ₂ R ₂ : 2-Fluoropyridyl	374 ± 170	0.3 ± 0.1
2e	R ₁ : Tetrahydro-4-pyranyl CH ₂ R ₂ : 2-Fluoroethyl	228 ± 54	1.1 ± 0.5
3l	R ₁ : CH ₂ CH ₂ OCH ₂ CH ₂ F R ₂ : Ethyl	>10 000	18.1 ± 7.2

The measurements were conducted on membrane fractions prepared from CHO cells expressing hCB1 or hCB2 receptors and the inhibition constants (K_i) of the ligands were determined using the Cheng–Prusoff equation.⁴⁷ The binding affinity data were in good agreement with the functional activity measurements, as all the ligands were found to have low nanomolar binding affinities at CB2 (Table 4). In general, the binding affinities were comparable to those of the CB2 PET-radioligands reported so far, e.g. [¹¹C]A-836339 (K_i = 0.6 nM), [¹⁸F]-MA3 (K_i = 0.8 nM) and [¹¹C]NE40 (K_i = 9.6 nM).^{21,25,27}

Radiolabelling of the pyridyl sulfone ligands

^{18}F -Fluorination of pyridyl derivatives was first trialled with trimethylammonium- and chloro-leaving groups (Scheme 4). Precursor **14d** was prepared in two steps: **1d** underwent $\text{S}_{\text{N}}\text{Ar}$ substitution with dimethylamine and the product was subsequently *N*-methylated to afford the trimethylammonium salt **14d**. 2-Chloropyridine precursors (**15d**, **15e** and **15g**) were prepared from the protected aryl sulfide intermediates **7d**, **7e** and **7j** following the same chemical conversions as described in the Scheme 2. Deprotection followed by Pd-catalysed C–S-coupling with 2-chloro-4-bromopyridine gave the biaryl sulfides that were then oxidised to the corresponding sulfones **15d**, **15e** and **15g**.

Low activity radiolabelling test reactions were carried out with dried ^{18}F - $[\text{K}(\text{K}_{2.2.2})]\text{F}$ complex in DMSO at 105 °C and at 130 °C for 15 min, using precursor **14d** or **15d**, respectively. Lower reaction temperature was chosen for the trimethylammonium precursor, as ammonium salts have a rather poor stability in higher temperatures.⁴⁸ The incorporation of $^{18}\text{F}\text{F}^-$ was found to be very similar in these reactions – 65% and 70% for **14d** and **15d**, respectively, which is rather surprising given the poorer leaving group ability of the chloride in the pyridine $\text{S}_{\text{N}}\text{Ar}$.⁴⁹ However, the dimethylamino side product, formed by reverse Menschutkin reaction⁴⁸ from **14d**, had a very similar retention time to the product ^{18}F -**1d**, which complicated the purification process. Based on the test reactions, we chose chloro as the leaving group for the further radiolabelling.

The radiosynthesis of ^{18}F -**1d** was fully automated onto the Synthra RN plus module. Radioactive yields of the reactions were calculated based on the activity measurement at the start of synthesis. The synthesis was tested with 20–41 GBq of starting activity, which afforded ^{18}F -**1d** with high, isolated radioactive yield ($24 \pm 5\%$ at EOS, non-decay corrected, $n = 8$). The yield was sufficient for the preclinical production of ^{18}F -**1d** and was not further optimised. Radiochemical purity of the formulated product was analysed to be >99%, and the product was confirmed to be stable for 4 hours in 10% ethanol/saline

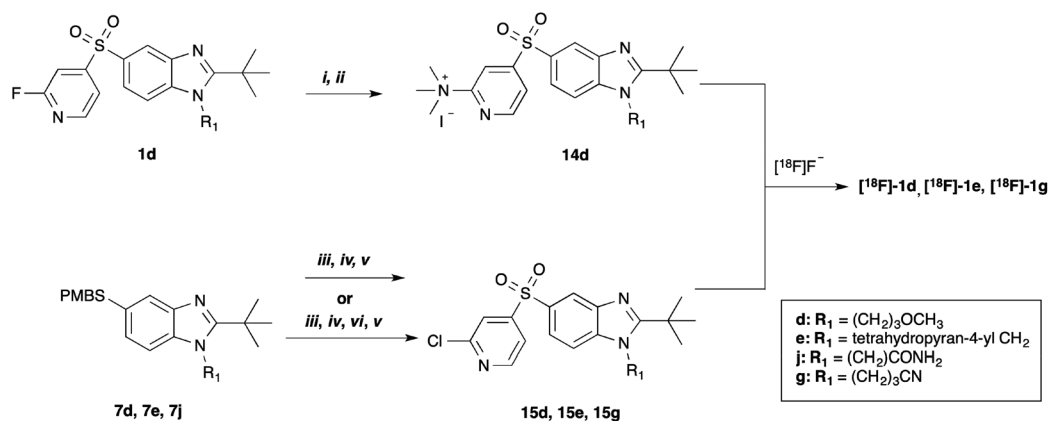
(0.9%). Using the same method, the other tracer candidates ^{18}F -**1e** and ^{18}F -**1g** were produced in $26 \pm 6\%$ ($n = 3$) and 28% ($n = 1$) isolated, radioactive yields (EOS, n.d.c.) with high radiochemical purity (>99%). The molar activities of ^{18}F -**1d**, ^{18}F -**1e** and ^{18}F -**1g** were measured to be $263 \pm 56 \text{ GBq } \mu\text{mol}^{-1}$ ($n = 8$), $158 \pm 32 \text{ GBq } \mu\text{mol}^{-1}$ ($n = 3$) and $128 \text{ GBq } \mu\text{mol}^{-1}$ ($n = 1$), respectively, at the end of synthesis. The formulated products ^{18}F -**1e** and ^{18}F -**1g** were confirmed to be stable for up to 4 hours in a solution consisting of 10% ethanol in saline (0.9%) with 0.5% sodium ascorbate (w/v).

Radiolabelling of the ethyl sulfone ligands

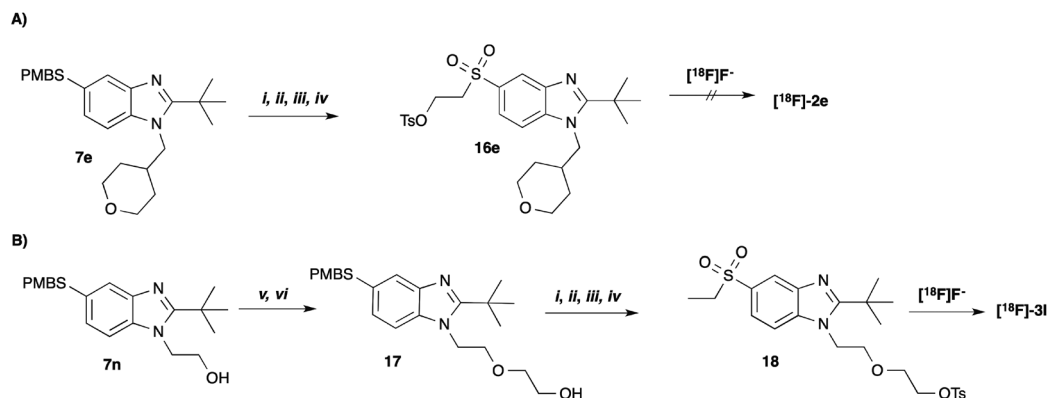
Precursor **16e** was prepared from the protected sulfide **7e** (Scheme 5A) according to the steps described earlier. After deprotection, the thiol intermediate was alkylated with 2-bromoethanol, and the resulting sulfide oxidised to sulfone. The pendant hydroxyl group was then reacted with tosyl chloride giving the labelling precursor **16e**. Precursor **18**, on the other hand, was prepared from the key alcohol intermediate **7n**. The chain was first extended by alkylation, followed by ester reduction to give the alcohol intermediate **17**. This was then subjected to tosylation to give the precursor **18**.

Attempts to radiolabel tosylate **16e** failed to give the desired product ^{18}F -**2e** (for details, see ESI†). Whilst our initial analysis of the ^{19}F -standard **2e** in 10% ethanol/saline (0.9%) indicated that this compound was stable for greater than 3 hours at room temperature, our subsequent studies confirmed that **2e** does completely degrade when subjected to the labelling conditions (1 mg mL^{-1} in DMF, $5 \mu\text{mol}$ of $\text{K}_{2.2.2}$, $5 \mu\text{mol}$ of K_2CO_3 , 150 °C, 5 min). It is possible that **2e** undergoes E1cb elimination in basic conditions at high temperature to form vinyl sulfone by-products. The observed instability of the target compound **2e** and the precursor **16e** sets limitations on reaction conditions and basicity of the reaction medium, and further optimisation would be required.

The radiolabelling of the precursor **18** was carried out in acetonitrile at 100 °C for 10 min resulting in high fluorine-18



Scheme 4 Synthesis of the labelling precursors **14d**, **15d**, **15e** and **15g**. Reagents and conditions: (i) *N,N*-Dimethylamine, DIPEA, ethanol, 80 °C (avg. 86%); (ii) CH_3I , CH_3OH , 40 °C (77%); (iii) TFA, 80 °C; (iv) 4-Br-2-Cl-pyridine, $\text{Pd}_2(\text{dba})_3$, Xantphos, Cs_2CO_3 , toluene, 100 °C (43–87% over two steps); (v) *m*-CPBA, DCM, 0 °C → RT (avg. 92%); (vi) TFAA, TEA, DCM, 0 °C → RT (75%).



Scheme 5 Synthesis of the tosylate precursors **16e** and **18** for the radiolabelling of ethyl sulfone derivatives. Reagents and conditions: (i) TFA, 80 °C; (ii) 2-bromoethanol or ethylbromide, TBAI, NaOH (aq.), MeOH, 60 °C (88–97% over two steps); (iii) *m*-CPBA, DCM, 0 °C → RT (avg. 92%); (iv) TsCl, pyridine, DMAP, DCM, 40 °C (40–43%); (v) 2-bromoacetic acid, NaH, TBAI, THF, 60 °C; MeOH, H₂SO₄, 60 °C (74% over two steps); (vi) DIBAL-H, THF, –78 °C → RT (avg. 88%).

incorporation yield of 74% (HPLC). These conditions were transferred to Synthra RNplus module, resulting in a high, isolated radioactive yield of [¹⁸F]-**3I** (43 ± 4%, n.d.c., *n* = 4) at the end of synthesis. However, the product was observed to undergo radiolysis with higher starting activities, and consequently, a lower starting activity (max. 6 GBq of [¹⁸F]fluoride)

and the use of Na-ascorbate as a radical scavenger was used for the final production runs. Na-Ascorbate was added in the HPLC-purification (0.5% w/v), SPE reformulation (5 mg mL⁻¹) and in the final formulated product (0.5% w/v). Radiochemical purity of the product [¹⁸F]-**3I** was found to be >97% and was observed to be stable for over two hours in the final formu-

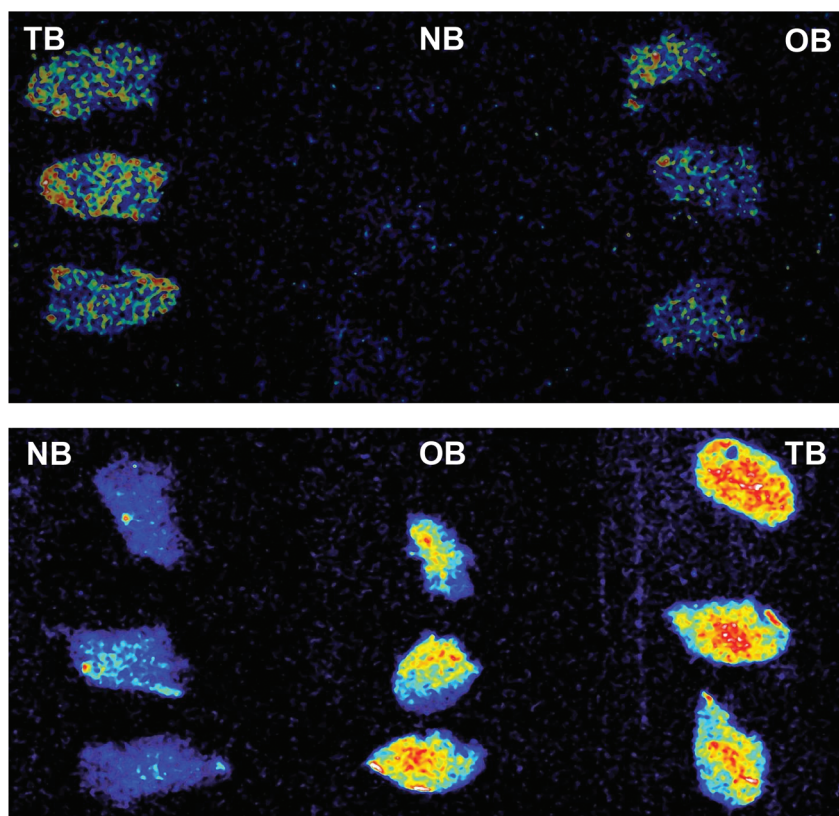


Fig. 2 Representative autoradiograms of rat spleen tissues after incubation with [¹⁸F]-**3I** (top) and [¹⁸F]-**1d** (bottom). TB = total binding; OB = off-target binding determined by co-incubation of the radioligands with GW-405833 (10 μM); NB = non-displaceable binding determined by co-incubation with ¹⁹F-standards **3I** and **1d** (10 μM).

lation. The molar activity of [^{18}F]-**3l** was measured to be $115 \pm 64 \text{ GBq } \mu\text{mol}^{-1}$ at the end of synthesis.

In vitro autoradiography

As a preliminary evaluation, the CB2-specific binding of two representative compounds, one from each ligand group [^{18}F]-**1d** and [^{18}F]-**3l**, was investigated using *in vitro* autoradiography on rat spleen that has a high level of CB2-receptors under basal conditions (Fig. 2).⁵⁰ Even though pyridyl sulfone [^{18}F]-**1e** had the highest CB2-affinity of the tested ligands, [^{18}F]-**1d** was selected, as it not only has high CB2-affinity ($K_i = 2.6 \pm 1.0 \text{ nM}$) but also excellent selectivity over CB1 subtype. CB2-specific binding was determined by incubating the radioligands in the presence of a known CB2-selective agonist GW-405833 (10 μM , $K_i \text{ rCB2} = 3.6 \pm 1.1 \text{ nM}$; $K_i \text{ rCB1} = 273 \pm 42.6 \text{ nM}$).⁵¹ Non-displaceable, non-specific binding was determined by co-incubation of the spleen sections with the radioligands and the corresponding ^{19}F -standards (10 μM). CB2-specific binding accounted for $32 \pm 14\%$ and $44 \pm 7\%$ of the total binding, whereas the non-displaceable binding was observed to be $34 \pm 10\%$ and $11 \pm 9\%$ of the total binding for [^{18}F]-**1d** and [^{18}F]-**3l**, respectively (1 σ). The CB2-specific component represented thus approximately 48% of the displaceable binding in both cases.

A few CB2-radioligands developed thus far, e.g. [^{11}C]-NE40 and [^{11}C]-RS-016, have shown high CB2-specific binding in murine spleen autoradiography *in vitro*.^{23,52} However, many CB2-radioligands have displayed high non-specific binding in spleen autoradiograms.^{53–55} For instance, high non-specific binding was reported for [^{18}F]-MA3, which was suggested to result from either suboptimal autoradiography protocol or a high k_{off} value of the radioligand.²⁷ Despite the inconclusive autoradiography data, [^{18}F]-MA3 was evaluated in a rat model with local striatal overexpression of hCB2, and was observed to show CB2-specific binding *in vivo*.²⁷ Whether the high off-target binding observed in rat spleen in this study translates into off-target binding in the brain in inflammatory conditions in other species, requires further evaluation.

Conclusions

In summary, a new series of fluorinated pyridyl and ethyl sulfonyl benzimidazole CB2-ligands were synthesised by varying the *N1*-alkyl chain. The ligands were found to be agonists with high efficacy, comparable to the standard CP-55940. Most of the ligands showed low nanomolar potency at CB2 and excellent subtype selectivity over the CB1 receptor. Based on the *in vitro* evaluation, the *N1*-area can be used for adjusting physicochemical properties of the ligands without losing activity, however, carboxylic acid or amide H-bond donor groups are not tolerated. The linear alkyl chains in the *N1*-area were observed to result in high CB2-selectivity. The ethyl sulfones showed, in general, slightly lower CB2 potency than 2-fluoropyridyl sulfones.

^{18}F -Labelled radiotracer candidates could be readily synthesised from 2-chloro pyridyl or alkyl tosylate precursors in high radiochemical yield and purity. In the *in vitro* autoradiography on rat spleen, CB2-specific binding of the selected radioligands accounted for 30–40% of the total binding, however, a substantial amount of the total binding was assigned to off-targets. Yet, the observed off-target binding may be highly dependent on species and organ/tissue under study, and may not translate into high CB2-unrelated binding in general or in the target organ brain. Thus, further *in vivo* evaluation of the CB2-radiotracer candidates presented here in a neuroinflammation model is warranted.

Experimental

The ESI† contains details of the chemical synthesis, radio-synthesis, HPLC-analytical conditions and experimental details of *in vitro* autoradiography and pharmacological assays.

Chemistry

Example of synthesis of compound **1a** *via* route A.

N-(2-Amino-5-((4-methoxybenzyl)thio)phenyl)pivalamide (5)

General method i. 5-Chloro-2-nitrobenzeneamine **4** (23 mmol, 4.0 g) was dissolved in ethanol (60 mL) under N_2 atmosphere. Potassium hydroxide (46 mmol, 2.6 g) and 4-methoxytoluene thiol (3.2 mL, 23 mmol) were added to the stirring solution that was then heated to mild reflux. After 2 h, reaction mixture was cooled down to room temperature and the yellow precipitate formed was filtered off. The solids were washed with small amount of ethanol. The crude product was dried under vacuum to give 5-((4-methoxybenzyl)thio)-2-nitroaniline as yellow crystalline solid that was used without purification for the next step.

General method ii. 5-((4-Methoxybenzyl)thio)-2-nitroaniline (3.0 g, 10 mmol) was weighed in a flask and dissolved in dry dichloromethane (50 mL) under N_2 atmosphere. Pyridine (1.2 mL, 16 mmol) and 4-dimethylaminopyridine (0.13 g, 10 mol%) were added to a stirring solution at room temperature. Pivaloyl chloride (1.5 mL, 1.2 equiv.) was added at RT, after which solution was heated to mild reflux overnight. Once the reaction was complete, the solution was diluted with DCM and water. Aqueous phase was extracted with DCM and combined organic phase was washed with 0.1 M HCl (25 mL) and brine. Crude product was dried over MgSO_4 and concentrated to give a solid that was purified on silica gel chromatography using gradient Hex \rightarrow EtOAc:Hex (1:9) \rightarrow EtOAc:Hex (1:5). This afforded *N*-(5-((4-methoxybenzyl)thio)-2-nitrophenyl)pivalamide as a light yellow crystalline solid (2.69 g, 72% over two steps).

M.p. 94.5 $^\circ\text{C}$; ^1H NMR (300 MHz, CDCl_3): δ 1.36 (9H, s), 3.79 (3H, s), 4.24 (2H, s), 6.85 (2H, d, $J = 7.5 \text{ Hz}$), 6.93 (1H, d, $J = 9 \text{ Hz}$), 7.33 (2H, d, $J = 7.8 \text{ Hz}$), 8.10 (1H, d, $J = 9 \text{ Hz}$), 8.90 (1H, s), 11.02 (1H, bs); ^{13}C NMR (75 MHz): δ 27.6 (3 \times C), 36.3, 40.9, 55.4, 114.3 (2 \times C), 116.8, 120.3, 126.1, 127.1, 130.4 (2 \times C),

132.7, 136.2, 150.6, 159.3, 178.4; HRMS (ESI-TOF) m/z calculated for $C_{19}H_{22}N_2O_4SN [M + Na]^+$ 397.1193, found 397.1194.

General method iii. *N*-(5-((4-Methoxybenzyl)thio)-2-nitrophenyl)pivalamide (2.00 g, 5.47 mmol) was weighed and dissolved in ethanol (50 mL) under N_2 atmosphere. The solution was heated to 40 °C. NH_4Cl (2.80 g, 10 equiv.) was dissolved in water (10 mL) and was added to the stirring solution. Iron powder (3.06 g, 10 equiv.) was added portionwise to a vigorously stirring solution. After 2 h, solution was cooled down to room temperature, and was diluted with DCM and water. Solution was filtered through a pad of basic alumina and Celite® and eluted with DCM/methanol mixture. Filtrate was concentrated and diluted with DCM. The aqueous layer was separated and the organic phase was washed with brine and dried over $MgSO_4$. Crude product was concentrated and dried under vacuum to give the title product (5) as light orange crystalline solid (1.65 g, 87%).

M.p. 124.8 °C; 1H NMR (300 MHz): δ 1.33 (9H, s), 3.78 (3H, s), 3.92 (2H, s), 6.68 (1H, d, $J = 8.4$ Hz), 6.79 (2H, d, $J = 8.1$ Hz), 7.01 (1H, d, $J = 8.1$ Hz), 7.10 (2H, d, $J = 8.4$ Hz), 7.14 (1H, s), 7.28 (1H, bs); ^{13}C NMR (75 MHz): δ 27.9 (3 × C), 39.5, 40.9, 55.4, 110.1, 113.9 (2 × C), 118.7, 124.8, 126.7, 129.9, 130.2 (2 × C), 131.9, 139.9, 158.7, 177.3; HRMS (ESI-TOF) m/z : calculated for $C_{19}H_{24}N_2O_2S [M + Na]^+$ 367.1451, found 367.1451.

***rac-N*-(5-((4-Methoxybenzyl)thio)-2-((2-methylpentyl)amino)phenyl)pivalamide (6a)**

General method iv. *N*-(2-Amino-5-((4-methoxybenzyl)thio)phenyl)pivalamide 5 (0.50 g, 1.46 mmol) was dissolved in dry DCM (25 mL) in a two-necked flask under N_2 atmosphere. *rac*-2-Methyl pentanal (0.2 mL, 1.6 mmol) and a few drops of glacial acetic acid were added to a stirring solution at room temperature. Solution was refluxed for 4 h, after which reaction was cooled down to room temperature. $NaBH_4$ (0.22 g, 4 equiv.) and MeOH (dry, 7 mL) were added gradually over 1.5 hours to a stirring solution at room temperature. After completion of the reaction, the mixture was diluted with water and DCM. The water layer was separated and extracted with DCM (3 × 20 mL). The combined organic phase was washed with brine and dried over $MgSO_4$. Purification on basic alumina using Hex → EtOAc : Hex (1 : 10) → (1 : 8) → (1 : 6) gave the title product as orange solid (0.39 g, 62%).

M.p. 72.9 °C; 1H NMR (300 MHz, $CDCl_3$): δ 0.91 (3H, t, $J = 6.9$ Hz), 0.98 (3H, d, $J = 6.6$ Hz), 1.20 (2H, m), 1.33 (9H, s), 1.40 (2H, m), 1.74 (1H, m), 2.86 and 2.97 (2H, 2 × dd, $J_1 = 6$ Hz, $J_2 = 11.7$ Hz), 3.77 (3H, s), 3.92 (2H, s), 6.64 (1H, d, $J = 8.4$ Hz), 6.79 (2H, d, $J = 8.4$ Hz), 7.08 (1H, m), 7.12 (2H, d, $J = 8.7$ Hz), 7.21 (1H, d, $J = 1.8$ Hz), 7.26 (1H, bs); ^{13}C NMR (75 MHz, $CDCl_3$): δ 14.4, 18.2, 20.2, 27.9, 32.9, 37.2, 39.5, 41.1, 50.6, 55.4, 110.1, 113.7, 113.8, 124.6, 130.15, 130.2 (2 × C), 130.4, 132.3, 142.7, 158.7, 177.4; HRMS (ESI-TOF) m/z : calculated for $C_{25}H_{36}N_2O_2SH [M + H]^+$ 429.2570, found 429.2571.

***rac*-2-(*tert*-Butyl)-5-((4-methoxybenzyl)thio)-1-(2-methylpentyl)-1*H*-benzo[*d*]imidazole (7a)**

General method v. *rac-N*-(5-((4-Methoxybenzyl)thio)-2-((2-methylpentyl)amino)phenyl)pivalamide (0.26 g, 0.60 mmol) was dissolved in toluene in a pressure flask and *p*-TsOH mono-

hydrate (0.17 g, 0.90 mmol) was added. Solution was heated to 130 °C in a sealed flask for over night. After completion of the reaction, solution was cooled down to room temperature and diluted with EtOAc. The organic phase was washed with saturated $NaHCO_3$ and brine, and dried over anhydrous $MgSO_4$. Filtration and concentration under reduced pressure gave the crude product that was purified on silica gel using EtOAc : Hex gradient (1 : 6 → 1 : 3) afforded the product as light yellow solid (0.17 g, 70%).

M.p. 78.1 °C; 1H NMR (300 MHz, $CDCl_3$): δ 0.97 (3H, d, $J = 6.9$ Hz), 0.99 (3H, t, $J = 6.6$ Hz), 1.38 (4H, m), 1.66 (9H, s), 2.42 (1H, m), 3.88 (3H, s), 4.17 (2H, s), 4.14–4.32 (2H, 2 × dd, $J = 7.2$ Hz, $J = 14.7$ Hz), 6.88 (2H, d, $J = 8.4$ Hz), 7.27 (4H, m), 7.93 (1H, s); ^{13}C NMR (75 MHz, $CDCl_3$): δ 14.3, 17.6, 20.2, 30.5 (3 × C), 33.5, 34.7, 37.1, 40.6, 51.7, 55.3, 110.8, 113.9 (2 × C), 122.7, 126.1, 128.3, 130.05 (2 × C), 130.15, 136.3, 142.4, 158.7, 162.0; HRMS (ESI-TOF) m/z : calculated for $C_{25}H_{34}N_2OS [M + H]^+$ 411.2465, found 411.2463.

***rac*-2-(*tert*-Butyl)-5-((2-fluoropyridin-4-yl)thio)-1-(2-methylpentyl)-1*H*-benzo[*d*]imidazole (8a)**

General method vi. *rac*-2-(*tert*-Butyl)-5-((4-methoxybenzyl)thio)-1-(2-methylpentyl)-1*H*-benzo[*d*]imidazole (83 mg, 0.20 mmol) was dissolved in trifluoroacetic acid (4 mL) and was refluxed at 80 °C for overnight. Reaction mixture was cooled down to room temperature and evaporated to dryness under N_2 flow. The resulting light yellow residue was used directly for the next step.

General method vii. A two-necked flask and a condenser were dried under vacuum with a heatgun and the system was left to cool down to room temperature under N_2 atmosphere. Toluene (4 mL) was added to the flask and degassed. Xantphos® (6 mg, 5 mol%) and $Pd_2(dba)_3$ (9 mg, 5 mol%) were added to the flask and the mixture was degassed. 4-Bromo-2-fluoropyridine (21 μ L, 0.20 mmol) was added to the reaction. Lastly, the crude 2-(*tert*-butyl)-1-(2-methylpentyl)-1*H*-benzo[*d*]imidazole-5-thiol (in 3 mL toluene) and Cs_2CO_3 (98 mg, 0.3 mmol) were added. The reaction mixture was refluxed at 110 °C for over night. After completion of the reaction, the reaction was diluted with EtOAc and sat. $NaHCO_3$ and filtered through a pad of silica and Celite® with EtOAc. The organic phase was separated, dried over anhydrous $MgSO_4$, filtered and concentrated to give a residue that was purified on silica gel using EtOAc : Hex (1 : 6), which afforded the title product 8a as light yellow oil (50 mg, 65% over 2 steps).

1H NMR (300 MHz, $CDCl_3$): δ 0.89 (3H, t, $J = 6.9$ Hz), 0.92 (3H, d, $J = 8.1$ Hz), 1.31 (4H, m), 1.57 (9H, s), 2.33 (1H, m), 4.13 (1H, dd, $J_1 = 14.7$ Hz, $J_2 = 9.0$ Hz), 4.24 (1H, dd, $J_1 = 14.7$ Hz, $J_2 = 6.9$ Hz), 6.40 (1H, s), 6.81 (1H, d, $J_1 = 5.4$ Hz), 7.35 (1H, d, $J = 9.6$ Hz), 7.41 (1H, d, $J = 8.4$ Hz), 7.91 (1H, d, $J = 5.4$ Hz), 7.97 (1H, s); ^{13}C NMR (75 MHz, $CDCl_3$): δ 14.3, 17.7, 20.2, 30.5 (3 × C), 33.6, 34.9, 37.1, 51.9, 105.3 (1C, d, $J = 40.7$ Hz), 112.3, 118.1 (1C, d, $J = 3.7$ Hz) 119.9, 127.6, 129.1, 138.3, 142.9, 146.8 (1C, d, $J = 16.1$ Hz), 157.7 (1C, d, $J = 8.4$ Hz), 164.2 (1C, d, $J =$

237 Hz), 163.3; ^{19}F NMR (258 MHz): -68.8 (s); LRMS (ESI) m/z : estimated 386.21 $[\text{M} + \text{H}]^+$ and 408.19 $[\text{M} + \text{Na}]^+$; found 386.24 and 408.21, respectively; HRMS (ESI-TOF) m/z : calculated for $\text{C}_{22}\text{H}_{28}\text{FN}_3\text{S}$ $[\text{M} + \text{H}]^+$ 386.2061, found 386.2060.

rac-2-(tert-Butyl)-5-((2-fluoropyridin-4-yl)sulfonyl)-1-(2-methylpentyl)-1H-benzo[d]imidazole (1a)

General method x. rac-2-(tert-Butyl)-5-((2-fluoropyridin-4-yl)thio)-1-(2-methylpentyl)-1H-benzo[d]imidazole (50 mg, 0.13 mmol) was dissolved in dry DCM (4 mL) under N_2 flow. *m*-CPBA (77%, 64 mg, 0.29 mmol) was added gradually at 0 °C. Once complete, the reaction was diluted with DCM, and aqueous sodium metabisulfate (5%, 4 mL) and sat. NaHCO_3 (5 mL) were added. The organic phase was washed with sat. NaHCO_3 (2 × 5 mL) and brine (5 mL), and was dried over anhydrous MgSO_4 . Filtration and concentration under reduced pressure gave the crude material that was purified on silica gel using EtOAc:Hex (1 : 6 → 1 : 4) gave the product **1a** as yellow viscous oil (42 mg, 78%).

^1H NMR (300 MHz, CDCl_3): δ 0.85 (3H, d, $J = 6.6$ Hz), 0.86 (3H, t, $J = 6.9$ Hz), 1.35 (4H, m), 1.55 (9H, s), 2.28 (1H, m), 4.18 (1H, dd, $J_1 = 14.7$ Hz, $J_2 = 6.9$ Hz), 4.18 (1H, dd, $J_1 = 14.7$ Hz, $J_2 = 9$ Hz), 7.41 (1H, m), 7.44 (1H, d, $J = 8.7$ Hz), 7.65 (1H, dt, $J_1 = 5.1$ Hz, $J_2 = 1.5$ Hz), 7.75 (1H, dd, $J_1 = 8.7$ Hz, $J_2 = 1.8$ Hz), 8.35 (1H, d, $J = 5.4$ Hz), 8.37 (1H, d, $J = 1.8$ Hz); ^{13}C NMR (75 MHz, CDCl_3): δ 14.2, 17.6, 20.2, 30.3 (3 × C), 33.7, 35.1, 37.0, 52.0, 108.0 (1C, d, $J = 40.2$ Hz), 111.8, 118.8 (1C, d, $J = 5.0$ Hz), 121.1, 121.5, 131.9, 141.0, 141.8, 149.5 (1C, d, $J = 14.4$ Hz), 156.1 (1C, d, $J = 6.6$ Hz), 163.8 (1C, d, $J = 242.6$ Hz), 165.1; ^{19}F NMR (282 Hz): δ -63.4 (s); HRMS (ESI-TOF) m/z : $[\text{M} + \text{Na}]^+$ calculated for $\text{C}_{22}\text{H}_{28}\text{FN}_3\text{O}_2\text{S}$ 440.1779, found 440.1778; HPLC-purity: >99%, RT = 23.6 min.

Conflicts of interest

The authors declare no competing financial interest.

References

- R. Ransohoff, *Science*, 2016, **353**, 777–783.
- M. T. Heneka, M. J. Carson, J. El Khoury, G. E. Landreth, F. Brosseron, D. L. Feinstein, A. H. Jacobs, T. Wyss-Corey, J. Vitorica, R. M. Ransohoff, K. Herrup, S. A. Frautschy, B. Finsen, G. C. Brown, A. Verkhratsky, K. Yamanaka, J. Koistinaho, E. Latz, A. Halle, G. C. Petzold, T. Town, D. Morgan, M. L. Shinohara, V. H. Perry, C. Holmes, N. G. Bazan, D. J. Brooks, S. Hunot, B. Joseph, N. Deigendesch, O. Garaschuk, E. Boddeke, C. A. Dinarello, C. J. Breitner, G. M. Cole, D. T. Golenbock and M. P. Kummer, *Lancet Neurol.*, 2015, **14**, 388–405.
- G. Martino, L. Adorini, P. Rieckmann, J. Hillert, B. Kallmann, G. Comi and M. Filippi, *Lancet Neurol.*, 2002, **1**, 499–509.
- J. W. Finnie, *Inflammopharmacology*, 2013, **21**, 309–320.
- J. D. Cherry, J. A. Olschowka and J. K. O'Banion, *J. Neuroinflammation*, 2014, **11**, 1–15.
- J. A. Kabba, Y. Xu, H. Christian, W. Ruan, K. Chenai, Y. Xiang, L. Zhang, J. M. Saavedra and T. Pang, *Cell. Mol. Neurobiol.*, 2018, **38**, 53–71.
- R. M. Ransohoff, *Nat. Neurosci.*, 2016, **19**, 987–991.
- C. Cerami, L. Iaccarino and D. Perani, *Int. J. Mol. Sci.*, 2017, **18**, 1–14.
- B. Pulli and J. W. Chen, *J. Clin. Cell. Immunol.*, 2014, **5**, 1–44.
- B. Janssen, D. J. Vugts, U. Funke, G. T. Molenaar, P. S. Kruijer, B. N. van Berckel, A. A. Lammertsma and A. D. Windhorst, *Biochim. Biophys. Acta*, 2016, **1862**, 425–441.
- S. Lavis, M. Guillemier, A. S. Hérard, F. Petit, M. Delahaye, N. Van Camp, L. Ben Haim, V. Lebon, P. Remy, F. Dollé, T. Delzescaux, G. Bonvento, P. Hantraye and C. Escartin, *J. Neurosci.*, 2012, **32**, 10809–10818.
- C. Wimberley, S. Lavis, V. Brulon, M. A. Peyronneau, C. Leroy, B. Bodini, P. Remy, B. Stankoff, I. Buvat and M. Bottlaender, *J. Nucl. Med.*, 2018, **59**, 307–314.
- D. R. Owen, A. J. Yeo, R. N. Gunn, K. Song, G. Wadsworth, A. Lewis, C. Rhodes, D. J. Pulford, I. Bennacef, C. A. Parker, P. L. StJean, L. R. Cardon, V. E. Mooser, P. M. Matthews, E. A. Rabiner and J. P. Rubio, *J. Cereb. Blood Flow Metab.*, 2012, **32**, 1–5.
- W. C. Kreisl, K. J. Jenko, C. S. Hines, C. H. Lyoo, W. Corona, C. L. Morse, S. S. Zoghbi, T. Hyde, J. E. Kleinman, V. W. Pike, F. J. McMahon and R. B. Innis, *J. Cereb. Blood Flow Metab.*, 2012, **33**, 53–58.
- D. R. Owen, R. N. Gunn, E. A. Rabiner, I. Bennacef, M. Fujita, W. C. Kreisl, R. B. Innis, V. W. Pike, R. Reynolds, P. M. Matthews and C. A. Parker, *J. Nucl. Med.*, 2011, **52**, 24–32.
- K. Maresz, E. J. Carrier, E. D. Ponomarev, C. J. Hillard and B. N. Dittel, *J. Neurochem.*, 2005, **95**, 437–445.
- G. A. Cabral and F. Marciano-Cabral, *J. Leukocyte Biol.*, 2005, **78**, 1192–1197.
- T. Hosoya, D. Fukumoto, T. Kakiuchi, S. Nishiyama, S. Yamamoto, H. Ohba, H. Tsukada, T. Ueki, K. Sato and Y. Ouchi, *J. Neuroinflammation*, 2017, **14**, 1–9.
- Y. Wang, X. Yue, D. O. Kiesewetter, G. Niu, G. Teng and X. Chen, *Eur. J. Nucl. Med. Mol. Imaging*, 2014, **41**, 1440–1449.
- I. Israel, A. Ohsiek, E. Al-Momani, C. Albert-Weissenberger, C. Stetter, S. Mencl, A. K. Buck, C. Kleinschnitz, S. Samnick and A.-L. Sirén, *J. Neuroinflammation*, 2016, **13**, 1–13.
- R. Ahmad, M. Koole, N. Evens, K. Serdons, A. Verbruggen, G. Bormans and K. Van Laere, *Mol. Imaging Biol.*, 2013, **15**, 384–390.
- R. Ahmad, A. Postnov, G. Bormans, J. Versijpt, M. Vandenbulcke and K. Van Laere, *Eur. J. Nucl. Med. Mol. Imaging*, 2016, **43**, 2219–2227.
- R. Slavik, A. Müller Herde, D. Bieri, M. Weber, R. Schibli, S. D. Krämer, S. M. Ametamey and L. Mu, *Eur. J. Med. Chem.*, 2015, **92**, 554–564.

- 24 R. Slavik, U. Grether, A. Müller Herde, L. Gobbi, J. Fingerle, C. Ullmer, S. D. Krämer, R. Schibli, L. Mu and S. M. Ametamey, *J. Med. Chem.*, 2015, **58**, 4266–4277.
- 25 G. Pottier, V. Gómez-Vallejo, D. Padro, R. Boisgard, F. Dollé, J. Llop, A. Winkeler and A. Martín, *J. Cereb. Blood Flow Metab.*, 2017, **37**, 1163–1178.
- 26 S. Yrjölä, M. Sarparanta, A. J. Airaksinen, M. Hytti, A. Kauppinen, S. Pasonen-Seppänen, B. Adinolfi, P. Nieri, C. Manera, O. Keinänen, A. Poso, T. J. Nevalainen and T. Parkkari, *Eur. J. Pharm. Sci.*, 2015, **67**, 85–96.
- 27 B. Attili, S. Celen, M. Ahamed, M. Koole, C. Van de Haute, W. Vanduffel and G. Bormans, *Br. J. Pharmacol.*, 2019, **176**, 1481–1491.
- 28 F. Spinelli, L. Mu and S. M. Ametamey, *J. Labelled Compd. Radiopharm.*, 2018, **61**, 299–308.
- 29 M. Aghazadeh Tabrizi, P. G. Baraldi, P. A. Borea and K. Varani, *Chem. Rev.*, 2016, **116**, 519–560.
- 30 G. Navarro, P. Morales, C. Rodríguez-Cueto, J. Fernández-Ruiz, N. Jagerovic and R. Franco, *Front. Neurosci.*, 2016, **10**, 1–11.
- 31 C. Turcotte, M. R. Blanchet, M. Laviolette and N. Flamand, *Cell. Mol. Life Sci.*, 2016, **73**, 4449–44470.
- 32 T. Cassano, S. Calcagnini, L. Pace, F. De Marco, A. Romano and S. Gaetani, *Front. Neurosci.*, 2017, **11**, 1–10.
- 33 T. Kato, K. Kon-I, Y. Yuki and K. Ando, Pfizer Inc., WO2007102059A1, 2007.
- 34 H. J. M. Gijzen, M. A. J. De Cleyn, M. Surkyn and B. M. P. Verbist, Janssen Pharmaceutica, WO2008003665A1, 2008.
- 35 C. Watson, D. R. Owen, D. Harding, K. Kon-I, M. L. Lewis, H. J. Mason, M. Matsumizu, T. Mukaiyama, M. Rodríguez-Lens, A. Shima, M. Takeuchi, I. Tran and T. Young, *Bioorg. Med. Chem. Lett.*, 2011, **21**, 4284–4287.
- 36 A. N. French, E. Napolitano, H. F. V. Brocklin, R. N. Hanson, M. J. Welch and J. A. Katzenellenbogen, *J. Labelled Compd. Radiopharm.*, 1991, **30**, 431–433.
- 37 A. N. French, E. Napolitano, H. F. V. Brocklin, R. N. Hanson, M. J. Welch and J. A. Katzenellenbogen, *Nucl. Med. Biol.*, 1993, **20**, 31–47.
- 38 M. A. Phillips, *J. Chem. Soc.*, 1928, 2393–2399.
- 39 V. W. Pike, *Curr. Med. Chem.*, 2016, **23**, 1818–1869.
- 40 S. A. Hitchcock and L. D. Pennington, *J. Med. Chem.*, 2006, **49**, 7559–7583.
- 41 B. M. P. Verbist, M. A. J. De Cleyn, M. Surkyn, E. Fraiponts, J. Aerssens, M. J. M. A. Nijssen and H. J. M. Gijzen, *Bioorg. Med. Chem. Lett.*, 2008, **18**, 2574–2579.
- 42 J. M. Frost, M. J. Dart, K. R. Tietje, T. R. Garrison, G. K. Grayson, A. V. Daza, O. F. El-Kouhen, B. B. Yao, G. C. Hsieh, M. Pai, C. Z. Zhu, P. Chandran and M. D. Meyer, *J. Med. Chem.*, 2010, **53**, 295–315.
- 43 S. D. Banister, J. Stuart, R. C. Kevin, A. Edington, M. Longworth, S. M. Wilkinson, C. Beinat, A. S. Buchanan, D. E. Hibbs, M. Glass, M. Connor, I. S. McGregor and M. Kassiou, *ACS Chem. Neurosci.*, 2015, **6**, 1445–1458.
- 44 M. Longworth, M. Connor, S. D. Banister and M. Kassiou, *ACS Chem. Neurosci.*, 2017, **8**, 1673–1680.
- 45 X.-Q. Xie, J. Z. Chen and E. M. Billings, *Proteins: Struct., Funct., Genet.*, 2003, **53**, 307–319.
- 46 V. M. Showalter, D. R. Compton, B. R. Martin and M. E. Abood, *J. Pharmacol. Exp. Ther.*, 1996, **278**, 989–999.
- 47 Y.-C. Cheng and W. H. Prusoff, *Biochem. Pharmacol.*, 1973, **22**, 3099–3108.
- 48 H. Sun and S. G. DiMagno, *J. Fluorine Chem.*, 2007, **128**, 806–812.
- 49 L. Dolci, F. Dollé, S. Jubeau, F. Vaufrey and C. Crouzel, *J. Labelled Compd. Radiopharm.*, 1999, **42**, 975–985.
- 50 S. J. Govaerts, E. Hermans and D. M. Lambert, *Eur. J. Pharm. Sci.*, 2004, **23**, 233–243.
- 51 K. Valenzano, L. Tafesse, G. Lee, J. E. Harrison, J. M. Boulet, S. L. Gottshall, L. Mark, M. S. Pearson, W. Miller, S. Shan, R. Rabadi, Y. Rotshteyn, S. M. Chaffer, P. I. Turchin, D. A. Elsemore, M. Toth, L. Koetzner and G. T. Whiteside, *Neuropharmacology*, 2005, **248**, 658–672.
- 52 N. Evens, C. Vandeputte, C. Coolen, P. Janssen, R. Sciote, V. Baekelandt, A. M. Verbruggen, Z. Debyser, K. V. Laere and G. M. Bormans, *Nucl. Med. Biol.*, 2012, **39**, 389–399.
- 53 L. Mu, R. Slavik, A. Müller, K. Popaj, S. Cermak, M. Weber, R. Schibli, S. D. Krämer and S. M. Ametamey, *Pharmaceuticals*, 2014, **7**, 339–352.
- 54 R. Slavik, A. Müller Herde, A. Haider, S. D. Krämer, M. Weber, R. Schibli, S. M. Ametamey and L. Mu, *J. Neurochem.*, 2016, **138**, 874–886.
- 55 R. Slavik, D. Bieri, S. Cermak, A. Müller, S. D. Krämer, M. Weber, R. Schibli, S. M. Ametamey and L. Mu, *Chimia*, 2014, **68**, 208–210.